



OPEN

The variability of functional MRI brain signal increases in Alzheimer's disease at cardiorespiratory frequencies

Timo Tuovinen^{1,2}✉, Janne Kananen^{1,2}, Zalan Rajna^{1,3}, Johannes Lieslehto⁴, Vesa Korhonen^{1,2}, Riikka Rytty^{1,5}, Heli Mattila^{1,2}, Niko Huotari^{1,2}, Lauri Raitamaa^{1,2}, Heta Helakari^{1,2}, Ahmed Abou Elseoud⁶, Johanna Krüger^{2,7}, Pierre LeVan^{8,9,10,11}, Osmo Tervonen^{1,2}, Juergen Hennig⁸, Anne M. Remes^{2,7}, Maiken Nedergaard¹² & Vesa Kiviniemi^{1,2}✉

Biomarkers sensitive to prodromal or early pathophysiological changes in Alzheimer's disease (AD) symptoms could improve disease detection and enable timely interventions. Changes in brain hemodynamics may be associated with the main clinical AD symptoms. To test this possibility, we measured the variability of blood oxygen level-dependent (BOLD) signal in individuals from three independent datasets (totaling 80 AD patients and 90 controls). We detected a replicable increase in brain BOLD signal variability in the AD populations, which constituted a robust biomarker for clearly differentiating AD cases from controls. Fast BOLD scans showed that the elevated BOLD signal variability in AD arises mainly from cardiovascular brain pulsations. Manifesting in abnormal cerebral perfusion and cerebrospinal fluid convection, present observation presents a mechanism explaining earlier observations of impaired glymphatic clearance associated with AD in humans.

The presence of aggregates of amyloid-beta (A β) protein and tau-protein in brain tissue are canonical pathologies of established Alzheimer's disease (AD)^{1,2}. The mechanism ultimately resulting in deposition of these aggregates remains unclear³, and the causal relationship between A β and tau deposition is debated⁴. The clinical diagnosis of AD is based on a battery of examinations, including neurological and neuropsychological tests, supplemented in recent years by structural MRI of the brain and metabolic imaging with FDG-PET^{5,6}. However, the diagnostic accuracy of available approaches is not completely satisfactory^{7,8}, and is especially problematic in early or prodromal phases of the disease⁹. In 2018, the National Institute on Aging and Alzheimer's Association of the United States proposed a shift of the diagnostic paradigm away from clinical symptoms or post mortem findings, towards criteria based on some combination of biomarkers in living persons¹⁰. While there has been some success in developing diagnostic tests based on analysis of markers in cerebrospinal fluid (CSF)^{11,12}, the requirement for invasive sampling is especially onerous in this vulnerable and aged population. An ideal biomarker for diagnosis of incipient Alzheimer's disease would be minimally invasive and yet highly sensitive to the brain pathology occurring at an early disease stage, thus perhaps enabling timely interventions.

Age, cerebrovascular disease, and hypertension are among the known risk factors for AD⁷. Indeed, aggressive treatment of high blood pressure in prospective studies lowered the risk of conversion from mild cognitive impairment (MCI) to Alzheimer's dementia¹³. Thus, cardiovascular function bears some relationship with human

¹Oulu Functional Neuroimaging, Medical Imaging, Physics and Technology, University of Oulu, Oulu, Finland. ²Medical Research Center, Oulu University Hospital, Oulu, Finland. ³Center for Machine Vision and Signal Analysis, University of Oulu, Oulu, Finland. ⁴Center for Life Course Health Research, University of Oulu, Oulu, Finland. ⁵Department of Neurology, Hyvinkää Hospital, Helsinki University Hospital, Hyvinkää, Finland. ⁶Department of Diagnostic Radiology, Helsinki University Hospital, Helsinki, Finland. ⁷Research Unit of Clinical Neuroscience, Neurology, University of Oulu, Oulu, Finland. ⁸Department of Radiology, Medical Physics, Medical Center - University of Freiburg, Faculty of Medicine, University of Freiburg, Freiburg, Germany. ⁹Department of Radiology, Cumming School of Medicine, University of Calgary, Calgary, Canada. ¹⁰Department of Paediatrics, Cumming School of Medicine, University of Calgary, Calgary, Canada. ¹¹Hotchkiss Brain Institute and Alberta Children's Hospital Research Institute, University of Calgary, Calgary, Canada. ¹²Center for Translational Neuromedicine, University of Rochester Medical Center, Rochester, NY, USA. ✉email: timo.tuovinen@oulu.fi; vesa.kiviniemi@oulu.fi

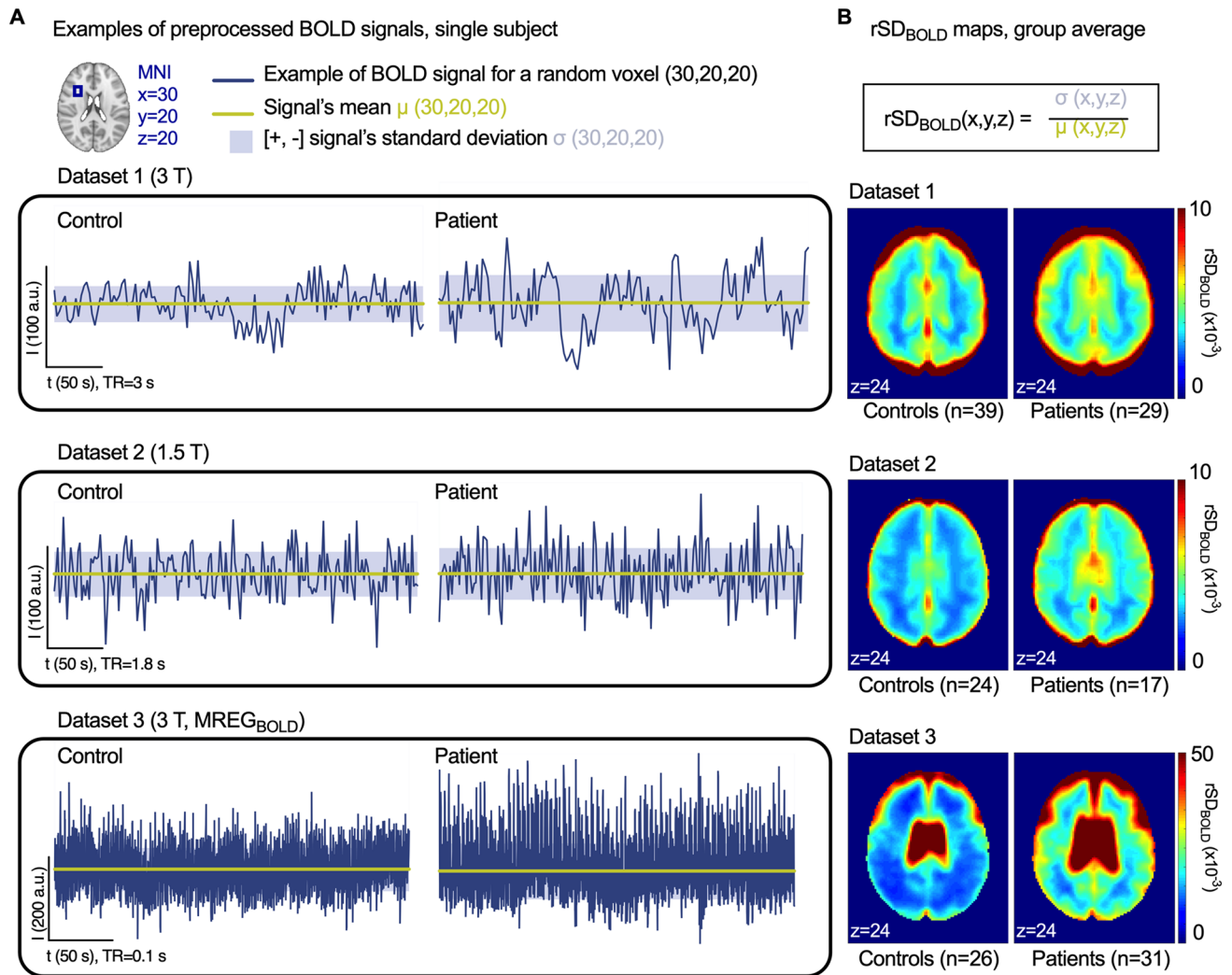


Figure 1. BOLD signal time series and formation of brain signal variability maps (rSD_{BOLD}) (A) Examples of random single voxel BOLD signals, the signal's mean and standard deviation for control subjects and AD patients from each dataset. Location of the random region-of-interest in MNI coordinates is shown in the group mean brain maps (B). As a measurement of brain signal variability, we calculated rSD_{BOLD} for each voxel and formed 3D maps.

AD pathophysiology. Cardiovascular pulsations in the brain parenchyma have been shown to drive the recently identified glymphatic clearance system of the brain, which utilizes perivascular spaces as channels to clear soluble proteins and various metabolites into the CSF and thence out of the central nervous system (CNS)^{14–16}. Notably in the present context of AD, the glymphatic system is the major pathway responsible for clearance of soluble A β from the brain interstitial fluid¹⁴. Aging, even in the absence of frank atherosclerosis, is associated with reduced elasticity of arterial walls, which leads to attenuation of glymphatic pulsation¹⁷. Similarly, increasing arterial blood pressure reduces pulsatility of the arterial wall, and reduces the net outflow of CSF along the perivascular spaces¹⁸. Thus, declining glymphatic function may be a factor in the accumulation of A β and other toxic aggregates associated with AD.

The blood oxygen level-dependent (BOLD) signal in functional MRI (fMRI) has mainly been used to measure very low frequency (VLF) hemodynamic responses to neuronal activity oscillations. However, the BOLD signal is also an indicator of basic underlying vascular and respiratory factors in the brain^{19–23}. Recent research has indicated an elevated variability in the BOLD signal, i.e. the relative standard deviation or coefficient of variation of the full band BOLD signal, in brain of AD patients^{24,25}. We hypothesized that the physiological brain pulsations driving the glymphatic clearance are altered in AD in a manner manifesting in increased variability in the brain BOLD signal. The objectives of this study were to (I) verify previous findings of altered brain BOLD signal variability in AD; (II) to develop a non-invasive MR-based biomarker for AD without requiring exogenous contrast agents; and (III) to study the physiological origin of the signal alteration. We examined three independent datasets from a total of 80 AD patients and 90 age-matched controls to evaluate brain signal variability reported as the relative standard deviation of the BOLD signal (rSD_{BOLD}) (Fig. 1). Using these datasets, we determined the replicability and effectiveness of rSD_{BOLD} in discriminating between AD patients and controls and confirmed

	Dataset 1	Dataset 2	Dataset 3
Scanner	Philips (13 sites)	GE Signa HDx	Siemens Skyra
Field strength (T)	3	1.5	3
Sequence	EPI	EPI	MREG, 3D spiral single shot
TR (ms)	3000	1800	100
TE (ms)	30	40	36
Duration (volumes/time)	140/7 min	202/6 min 4 s	2961/5 min
FA (deg)	80	90	25
Voxel size (mm)	4 × 4 × 4	3 × 3 × 3	3 × 3 × 3
Slice thickness (mm)	3.3	4	3
Matrix size	64 × 64	64 × 64	64 × 64

Table 1. Imaging parameters for functional data. TR = Repetition time. TE = Echo time. FA = Flip angle.

	Participants	Age (years)	Female	Disease duration (years)	MMSE	Average fMRI datasets per participant
Dataset 1 (ADNI)						
AD patients	29	71.7 ± 6.5	14 (48%)	NC	21.8 ± 3.6 * [12–28]	2.1 [1–3]
Controls	39	72.7 ± 4.3	25 (62%)	-	29.1 ± 1.3 [24–30]	2.2 [1–3]
Dataset 2 (local)						
AD patients	17	60 ± 5.4	11 (65%)	2.6 ± 1.3	22.9 ± 2.6 * [18–27]	1
Controls	24	60.0 ± 5.1	12 (50%)	-	29.0 ± 1.1 [26–30]	1
Dataset 3 (local)						
AD patients	31	60.5 ± 4.8 *	18 (58%)	3.4 ± 2.3	22.3 ± 6.3 * [10–30]	1
Controls	26	57.3 ± 5.7	16 (62%)	-	28.6 ± 1.2 * [25–30]	1

Table 2. Participant demographics. Descriptive demographic characteristics of the groups. Values represent mean ± SD or N (%). [Range]. NC = Not collected, multiple datasets. MMSE = Mini Mental State Examination (maximum total score is 30). * patients versus controls, where $P < 0.05$.

the longitudinal repeatability of rSD_{BOLD} for AD detection. Finally, we used ultrafast functional MRI scanning in the third dataset ($MREG_{BOLD}$) with physiological data of cardiopulmonary function to test our hypothesis that increased BOLD signal variability is more related to physiological mechanisms driving the glymphatic brain clearance than an indicator of VLF fluctuations of the BOLD signal arising from perturbed neuronal activity.

Results

We used data from a sample of 80 AD patients and 90 healthy controls compiled from three independent datasets (two local and one from International Alzheimer’s disease Neuroimaging Initiative ADNI), who were imaged without exogenous contrast agents using either conventional or fast fMRI (Table 1). After conventional preprocessing and quality control of the imaging data, BOLD signal sequences from 89 healthy controls and 77 AD patients were eligible for analysis. Demographics and clinical data of the included participants are summarized in Table 2. We used the relative standard deviation of the BOLD signal (rSD_{BOLD}) to measure brain signal variability^{26–28} (Fig. 1). rSD_{BOLD} is also known as the coefficient of temporal variation (CV), where a higher CV value equals greater variability of amplitude of the BOLD signal.

Brain signal variability is increased in AD. In whole brain voxel-wise analysis, AD patients showed increased rSD_{BOLD} ($P < 0.05$, corrected for multiple comparisons, and with head motion parameters used as a regressor) in clusters of voxels distributed around the basal ganglia and in the white matter around lateral ventricles (Fig. 2 and S1). These clusters were defined as regions-of-interest (ROIs) for further analysis ($ROI_{dataset1-3}$). There were no regions with significantly higher rSD_{BOLD} in controls relative to the patients. We further used voxel-based morphometry (VBM) to compare patterns of neurodegeneration with the regional rSD_{BOLD} changes. The extent of gray matter atrophy in the AD group was in line with the previous literature^{5,29} and had only partial overlap with the clusters of increased rSD_{BOLD} (Figs. S1, S2).

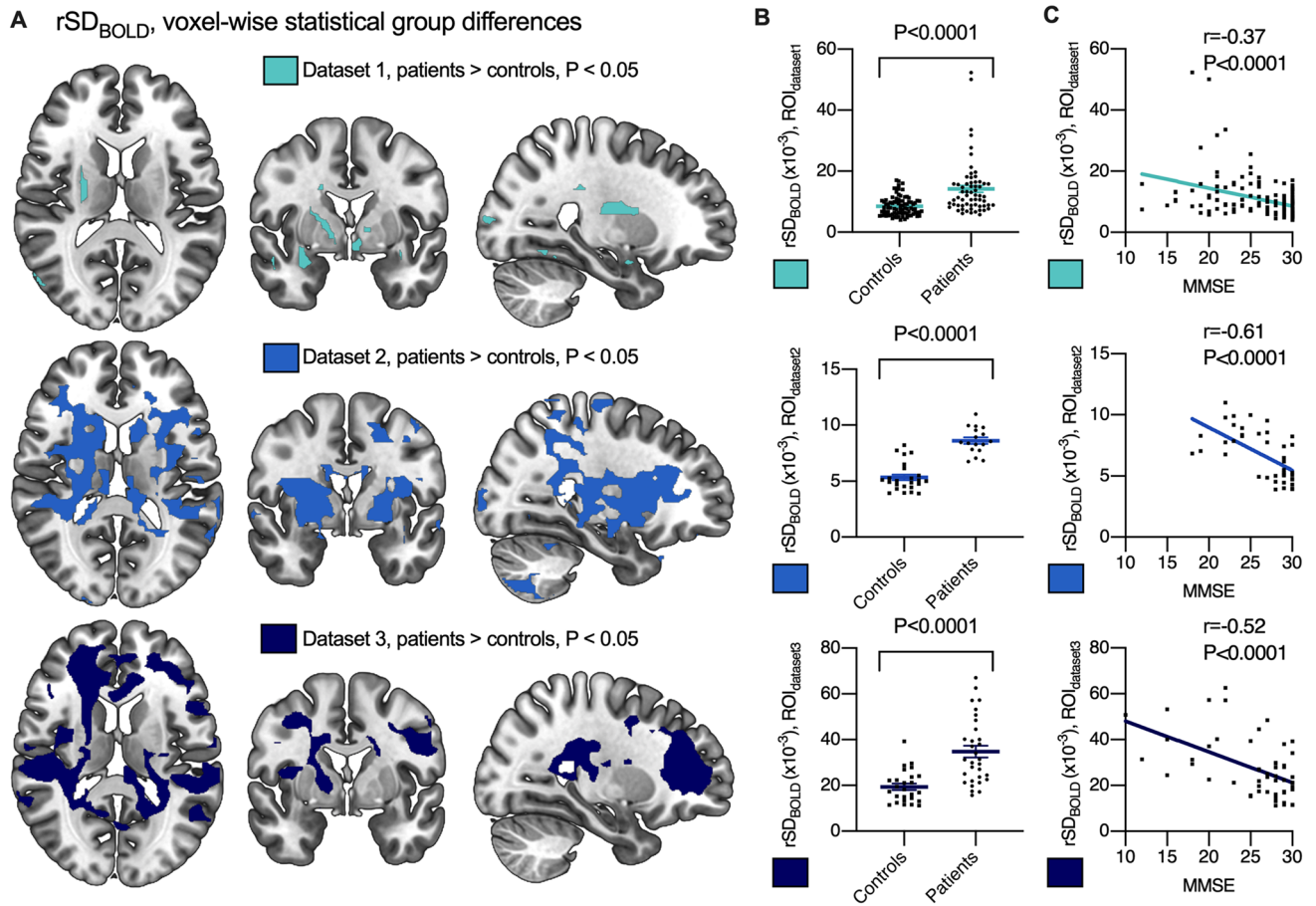


Figure 2. Brain BOLD signal variability in patients with AD compared with controls. Differences in rSD_{BOLD} according to whole-brain voxel-wise analyses (A). Maps represent group-level differences where rSD_{BOLD} is higher in Alzheimer's disease patients ($P < 0.05$, family wise error corrected). These maps are used as region-of-interests ($ROI_{dataset1}$, $ROI_{dataset2}$, $ROI_{dataset3}$) in further analysis. (B) chart shows the mean \pm standard error of the mean rSD_{BOLD} values to group, extracted from each $ROI_{dataset1-3}$ e.g. significant clusters determined in A. (C) shows correlation between rSD_{BOLD} and Mini-Mental State Examination (MMSE).

Brain signal variability increase is associated with declined MMSE. The Mini-Mental State Examination (MMSE) was used to test for cognitive impairment in the participants (Table 2). MMSE scores range from 0 to 30, with a score of 10 to 26 indicating mild-to-moderate cognitive impairment³⁰. There was negative correlation with MMSE and average rSD_{BOLD} within ROIs from each of the three datasets ($r = -0.37$ to -0.61 ; $P < 0.0001$), meaning that increased BOLD signal variability was associated with lower cognitive function scores (Fig. 2C).

Replicability of brain signal variability increase. First, present results replicated previous findings of increased BOLD signal variability in AD patients compared to controls^{24,25}. We next assessed the anatomical concordance of the regions of increased rSD_{BOLD} in the three independent AD datasets in this study. There were altogether 948 common voxels (7.6 cm^3) that showed significantly increased rSD_{BOLD} in all three datasets. The anatomical patterns of statistically significant changes in rSD_{BOLD} were markedly alike in all three datasets, despite the use of different imaging setups and parameters (Table 1, Figs. S1 and S2). Notably, scanning protocols differed with respect to sampling rate (repetition time, TR) (Fig. 1). The spatial extent of the rSD_{BOLD} increases in AD patients versus controls was larger in dataset 2 than in dataset 1, and larger still in dataset 3 (MREG_{BOLD}), which matched the rank order to the increasing sampling rates, i.e. faster temporal scanning. That association shows that the temporal resolution of the data is an important factor for the detection of AD-dependent rSD_{BOLD} alterations.

Accuracy and repeatability of brain signal variability in discriminating AD patients from controls. To our knowledge, this is the first study to analyze diagnostic accuracy and repeatability of increased BOLD signal variability in AD. Receiver operating characteristic (ROC) curve and the area under the ROC curve (AUC) were calculated to establish the feasibility of using rSD_{BOLD} as a biomarker for AD. Dataset 2 (AUC = 0.81, $P = 0.0009$) and dataset 3 (AUC = 0.73, $P = 0.0034$) both demonstrated good effectiveness of the rSD_{BOLD} values within $ROI_{dataset1}$ in discriminating between AD patients and controls (Fig. 3A-C).

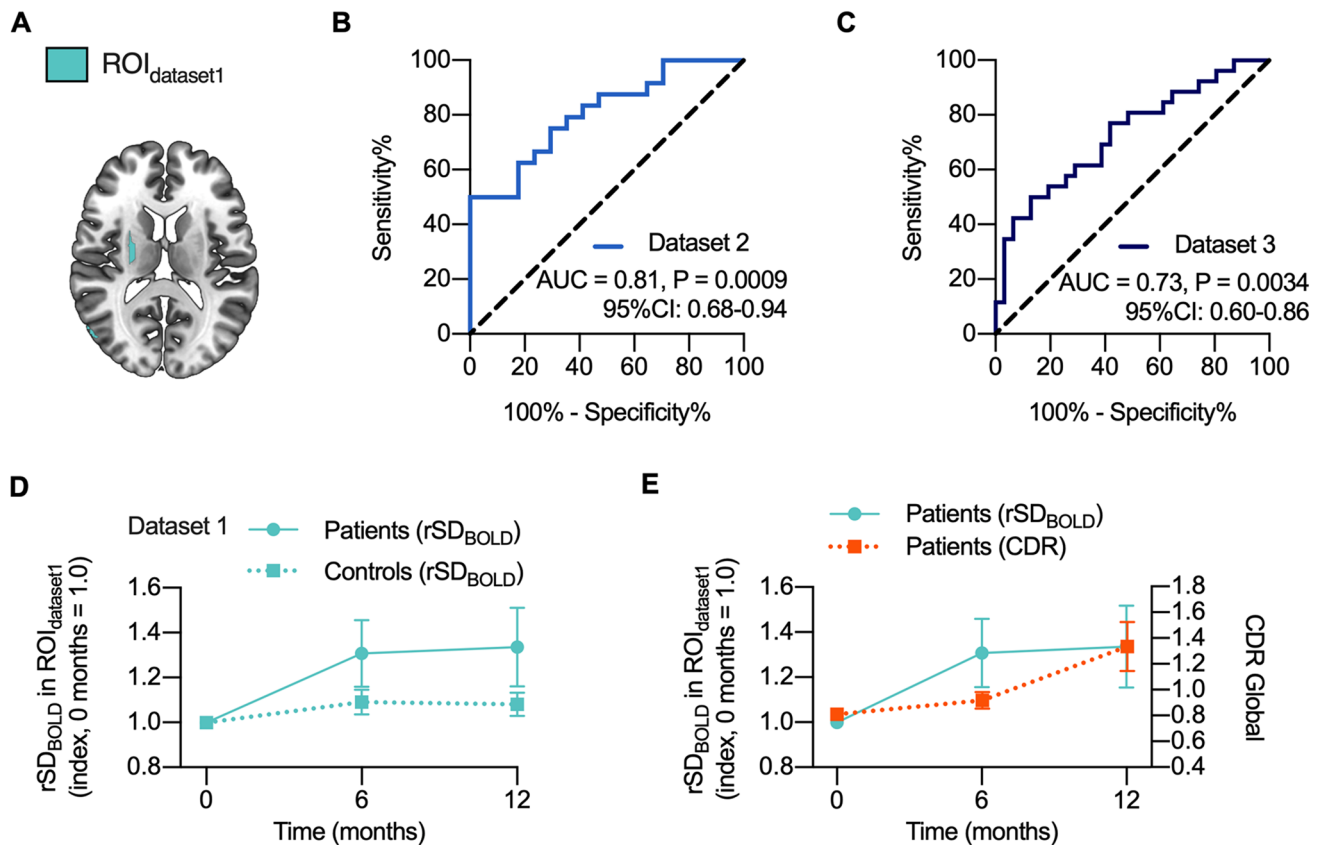


Figure 3. Accuracy and repeatability. (A) Region-of-interest (ROI_{dataset1}) was defined by significant clusters in dataset 1 (c.f. Figure 2A). Receiver operating characteristic (ROC) curves and area-under-curve (AUC) for differential diagnosis was based on mean rSD_{BOLD} values in datasets 2 (B) and 3 (C) within this ROI_{dataset1}. Confidence intervals and statistical significance are also shown. (D) Within-individual changes in the average rSD_{BOLD} in ROI_{dataset1} over time after baseline imaging (0 months) in AD patients and controls in dataset 1. There was statistical difference between the two groups at both 6 and 12 months. Data represents the mean \pm standard error of the mean. Mixed-effect analysis significance between groups $p < 0.035$ and between timepoints $p < 0.0054$ corrected for multiple comparison. Predicted mean increase was in AD 21% and in controls 5%. (E) presents indexed rSD_{BOLD} change and Clinical Dementia Rating (CDR) global values in follow up in patients.

To analyze the repeatability and possible effect of disease progression of these findings, we scrutinized the follow-up data in the dataset 1. In the control group average rSD_{BOLD} values within ROI_{dataset1} were relatively stable over a 12-month period (+8% on average, not significant) (Fig. 3D), thus indicating good repeatability. Importantly, the rSD_{BOLD} increased (+32% on average, $P = 0.0054$) *only* in the AD group ($P = 0.035$), while Clinical Dementia Rating (CDR) also increased in the patient group, denoting greater cognitive impairment (Fig. 3E), thus indicating a relationship between rSD_{BOLD} increases with disease progression.

Increased brain signal variability in cardiac and respiratory frequencies. We next asked whether BOLD signal variability is increased in AD patients due to changes in their hemodynamic responses to neuronal activity oscillations (at very low frequencies, VLF) or rather due to other fast physiological components of the BOLD signal, namely cardiac and respiratory pulsations. Previous pioneering work along these lines^{24,25}, as well as the datasets 1 and 2 in this study, employed relatively slow sampling rates (TR = 1.8–3.0 s, equivalent to 0.33–0.56 Hz). Thus, any signal with frequency content higher than the corresponding Nyquist rate would have been aliased into the BOLD signal, which is here the case for cardiac (0.8–1.65 Hz) and parts of the respiratory (0.15–0.4 Hz) signals.

Fast fMRI sequences enable the detection of physiological oscillations that propagate from cardiac and respiratory pulsations within their respective frequency sub-bands^{22,31,32}. We used an ultra-fast fMRI sequence (MREG_{BOLD}, dataset 3) sampled with TR 0.1 s, corresponding to ten complete brain acquisitions per second, to examine the variation within different frequency bands of the BOLD signal (Fig. 4A). We then calculated SD maps of the MREG_{BOLD} with bandpass filtration at physiological frequencies, aiming to discover the physiological source of increased rSD_{BOLD} in the AD group. Much as with rSD_{BOLD} maps of full band signal described above, we calculated the whole brain voxel-wise analysis of SD maps of bandpass-filtered MREG_{BOLD} for the AD and control groups (Fig. 4B).

We then compared the voxel-wise group-level difference between the AD and control groups in rSD maps of full band MREG_{BOLD} and in SD maps of cardiac (SD_{card}), respiratory (SD_{resp}), and VLF (SD_{VLF}) band data. This

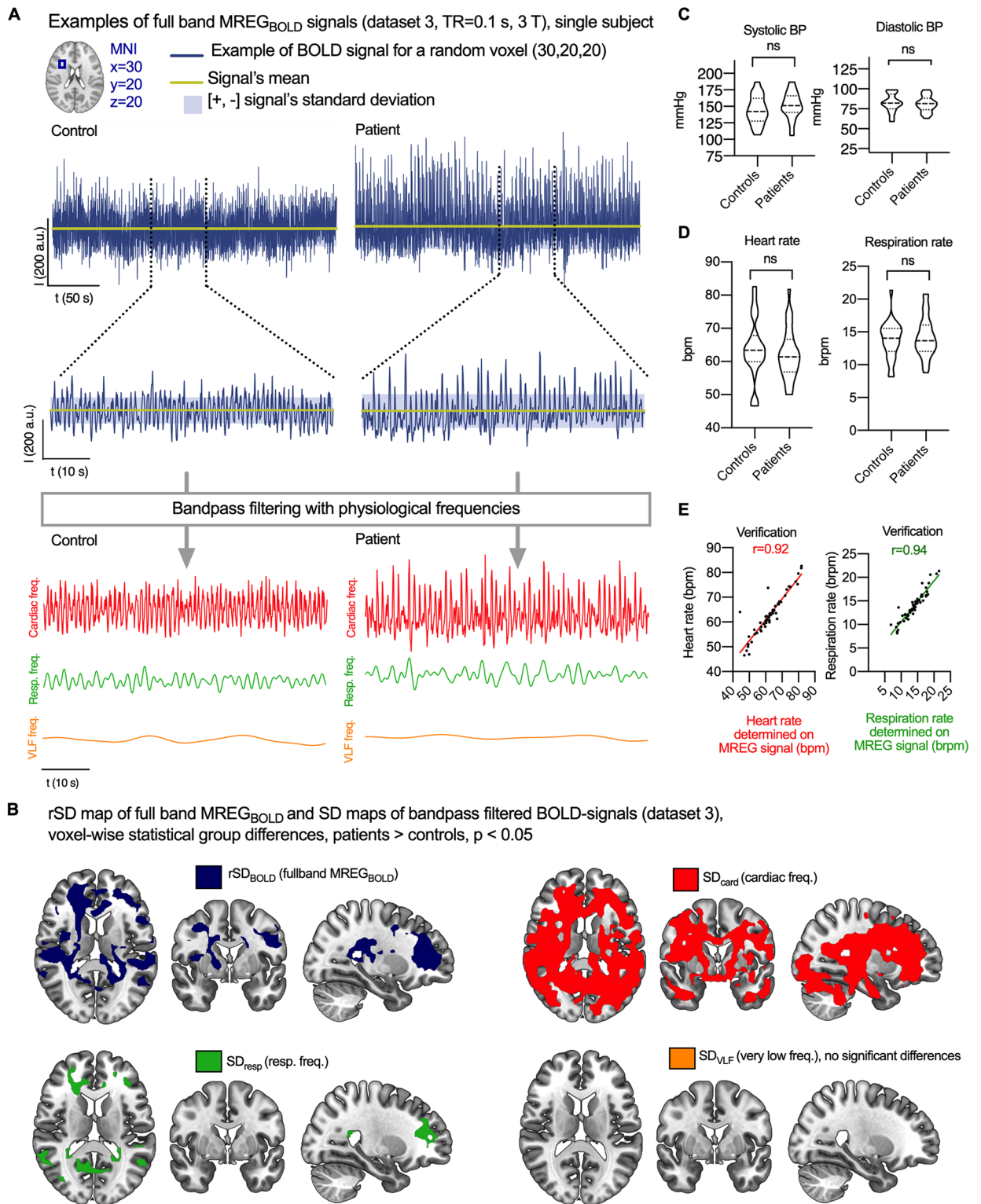


Figure 4. Physiological source mapping. (A) MREG_{BOLD} signal is imaged with fast sampling rate (TR = 0.1 s). A representative 60 s clip is shown for the purposes of illustration. MREG_{BOLD} signal is bandpass filtered to physiological frequencies to study the cardiac, respiratory and VLF parts of the signal. (B) Differences in rSD_{BOLD} and SD of bandpass filtered signals according to whole-brain voxel-wise analyses. Maps represent group-level differences where SD is higher in Alzheimer's disease patients ($P < 0.05$, family wise error corrected). (C) Blood pressure (BP) while supine just prior to entering the MR scanner. (D) Heart and respiration rates from peripheral pulse oximeter and respiration belt, respectively. (E) Heart and respiration rates determined on MREG signal and their correlation to peripheral signals. NS = not significant.

showed that rSD maps of the full band and SD maps of cardiac and respiratory parts of the signal overlapped spatially. Moreover, the SD_{card} showed widespread increases extending beyond the corresponding findings for full band rSD_{BOLD} in the AD group (Fig. 4B). Most areas adjacent to periventricular structures showed increased SD_{card} , especially in the posterior brain regions. The increased SD_{card} extended down from somatosensory areas and encompassed most of the periventricular white matter. Increased SD_{card} could also be discerned in the bilateral basal ganglia of AD patients, but there were no such changes in frontal, insular and visual cortex (Fig. 4). All the regions with elevated respiratory SD_{resp} overlapped with regions with increased SD_{card} .

The SD_{resp} maps indicated group differences in bilateral frontal and temporoparietal areas, left sensorimotor cortex, medial frontal and temporal gyri. Notably, the anterior and posterior corpus callosum and bilateral angular gyri of the default mode network both also had increased SD_{resp} in the AD group. Between-group voxel-wise differences in SD_{VLF} maps did not attain statistical significance ($P = 0.06-0.1$).

No difference in blood pressure, heart or respiration rate between patients and controls. To verify the nature of cardiac and respiratory signals, we used simultaneous within-subject cardio-respiratory data derived from peripheral heart rate pulse oximeter and respiratory belt measurements in dataset 3. Importantly, there were no between-group differences in heart or respiratory rate nor in the blood pressure, which was measured twice just before the scanning (Fig. 4C-D). We calculated average heart and respiratory rate from the $MREG_{BOLD}$ signal for each subject. These results had a strong positive correlation ($r = 0.92-0.94$, $P < 0.0001$) with the physiological verification data (Fig. 4E).

Discussion

Using three independent fMRI datasets, we confirmed previous findings that brain signal variability (rSD_{BOLD}) is increased in AD^{24,25}. ROC curve analysis results indicated that the rSD_{BOLD} has good precision for the differentiation of AD patients and controls. Indeed, the ROC AUC (0.73–0.81) by present methods is comparable to that reported in various invasive biomarker studies^{6,8,12}. Longitudinal follow-up data from the ADNI study showed that the rSD_{BOLD} measure is repeatable in controls but increases with time in individual AD patients scanned with one-year follow-up. This indicates an association between elevated rSD_{BOLD} and disease progression. Increased rSD_{BOLD} also correlated with lower MMSE values in all three datasets, denoting a general association with cognitive dysfunction. Our findings in the dataset with ultrafast $MREG_{BOLD}$ and simultaneous within-subject cardio-respiratory data shows that the physiological BOLD signal variability in AD patients originates predominantly from variability of cardiac pulsatility, and to a lesser degree respiratory signal variability.

Recent research indicates that the glymphatic brain clearance driven by physiological brain pulsations might be impaired in AD^{18,33,34}. The glymphatic influx of CSF tracers is driven by arterial wall pulsations driven by the cardiac cycle¹⁸, while other functional neuroimaging studies indicate that both the cardiovascular and the respiratory pulsations drive CSF convection^{22,32,35}. Our present use of fast $MREG_{BOLD}$ signals sampled at 10 Hz in dataset 3 enables exact separation of the cardiorespiratory pulsation from the low frequency BOLD signal without aliasing³⁶. We thus find that the increased brain BOLD signal variability in the AD group is mainly derived from or driven by cardiac frequency brain pulsations, which are also understood to be the main driver for glymphatic paravascular fluid transport¹⁸. The respiratory pulsations appear to play a lesser role in provoking the BOLD signal variability increase often detected in AD populations.

The peripheral cardiorespiratory measurements in the subjects from dataset 3 indicate that general features of cardiorespiratory physiology are insufficient to explain the increased intracranial BOLD signal variability in AD, as we note that the neither the average cardiorespiratory rates nor the blood pressure differed between the control and AD groups in that study. On the other hand, the cardiovascular pulse propagation *inside* the brain parenchyma has been found to be more variable in AD³⁷. Although the VLF fluctuations are normally the dominant source of variance in BOLD signal, we find that in AD, the main driver for this variability was brain pulsations arising from cardiac frequency.

There are some strengths and limitations that should be considered in the interpretation of the present results. First, there is a certain lack of standards in methodology and terminology in this area of research. A common issue in fMRI scanning has been the dependence of the results on scanner and imaging parameters. However, the concordance of present rSD_{BOLD} results from three independent datasets seems to indicate a consistent pattern of AD-related changes, despite quite substantial differences in the different vendor scanners and scanning parameters. The rSD_{BOLD} results are robust for a broad range of BOLD image sampling rates, this consistently indicating a source in physiological cardiopulmonary pulsations. Since results from conventional and ultrafast fMRI agree, both methods seem applicable for diagnostic purposes. However, larger replication samples with longitudinal fMRI measurements shall be required. Prospective studies of preclinical or prodromal AD with fMRI should serve to establish the diagnostic usefulness of present methods. As dementia is a clinical syndrome with variable manifestations and is often accompanied by neuropsychiatric and behavioral problems, further work with different patient groups is required to establish the viability of this method as a differential diagnosis tool²⁹.

In conclusion, we detected increased physiological BOLD signal variability in AD. The new index of rSD_{BOLD} may offer a non-invasive biomarker for diagnosis of AD without exogenous requiring CSF sampling or scanning in conjunction with MR contrast agents or nuclear imaging. Our results implicate altered intracranial cardiorespiratory pulsation as the driver for increased rSD_{BOLD} , which may help to tie together glymphatic clearance and pathophysiological mechanisms underlying AD. Future studies should investigate how rSD_{BOLD} is changed in other neuropathological conditions and during the course of MCI in a longitudinal study design with large patient cohorts. In addition, studies revealing a mechanistic relation between rSD_{BOLD} and other biomarkers such as A β and tau are required to understand the bigger picture of the underlying AD pathogenesis.

Materials and methods

Study design. The objectives of this study were to (I) verify previous findings of increased BOLD signal variability (rSD_{BOLD}) in AD, (II) to develop a non-invasive imaging biomarker for AD without requirement for exogenous MR contrast agents or ionizing radiation exposure; and (III) to study the physiological origin of the increased rSD_{BOLD} . We used a sample of 80 AD patients and 90 healthy controls derived from three independent datasets, one being the publicly available international multisite ADNI study (dataset 1), and two having been acquired at our institute (datasets 2–3). No power analysis was performed before the study; the dataset sizes were in line with previous experiments using functional imaging in patients with AD. Data collection and further analyses were not performed blind to the conditions of the experiment. However, preprocessing of neuroimaging data included standard automated analytic pipelines, which were agnostic to the diagnostic and demographic characteristics of the data.

Participants. All the patients of the AD groups met the NINCDS-ADRDA (National Institute of Neurological and Communicative Disorders and Stroke and the Alzheimer's Disease and Related Disorders Association) criteria for AD⁵. The control subjects were interviewed, and Mini-Mental State Examination (MMSE) and Beck's Depression Inventory (BDI) were performed to exclude any cases of dementia. Any psychiatric or neurological disorders or medications affecting the central nervous system were exclusion criteria for the control group.

As per ADNI protocols, all procedures performed in studies involving human participants were in accordance with the ethical standards of the institutional and/or national research committee and with the 1964 Helsinki declaration and its later amendments or comparable ethical standards. More details can be found at <http://adni.loni.usc.edu>. As per local data, written informed consent was obtained from all the participants or their legal guardians prior to scanning. The study was approved by the Regional Ethics Committee of the Northern Ostrobothnia Hospital District. Research was conducted accordance with Helsinki declaration.

Dataset 1 used in the preparation of this article was obtained from the ADNI database (<http://adni.loni.usc.edu>). ADNI was launched in 2003 as a public–private partnership, led by Principal Investigator Michael W. Weiner, MD. The primary goal of ADNI has been to test whether serial magnetic resonance imaging (MRI), positron emission tomography (PET), other biological markers, and clinical and neuropsychological assessment can be combined to measure the progression of mild cognitive impairment (MCI) and early AD. For up-to-date information, see <http://www.adni-info.org>. We selected ADNI-2 participants in whom resting state fMRI and preprocessed anatomical scans had been obtained within the first year of their participation in the study. One-year follow-up data was available from dataset 1. All the patients of the **datasets 2–3** had been examined by experienced neurologists specialized in memory disorders at the outpatient memory clinic of the Department of Neurology of Oulu University Hospital in Finland. The Finnish AD patients underwent a battery of examinations, including clinical and neurological examinations, screening laboratory tests, a neuropsychological examination and both structural and functional MRI of the brain. As required for clinical workup, CSF analyses of the biomarkers A β 42, tau and phospho-tau and/or functional neuroimaging by fluorodeoxyglucose positron emission tomography (FDG-PET) had been performed on the patients to confirm their diagnosis. All of the AD group patients met the current diagnostic criteria for AD⁵. The control subjects were interviewed, and Mini-Mental State Examination (MMSE) and Beck's Depression Inventory (BDI) were performed to screen for any individuals with memory deficits or depression. Any psychiatric or neurological disorders or use of medications affecting the central nervous system were exclusion criteria for the control group. There was no follow-up imaging data for the subjects in datasets 2–3.

After preprocessing and quality control of the three datasets, one control and three AD patients were excluded from the study owing to excessive head motion or other artifacts in the data, and one individual with AD was excluded because of the incidental finding of a brain tumor. A total of 89 healthy controls and 77 AD patients were eligible for analysis. Demographics and clinical data of the included participants are summarized in Table 2. There were no differences between the groups for age and sex demographics in datasets 1 and 2. In dataset 3, the AD patients were of slightly greater mean age ($P=0.02$).

Imaging data. Each subject was imaged for both functional and structural MRI. Details of the scanning parameters for the anatomical scans are shown in Supplement Table 1. Imaging parameters for functional MRI are shown in Table 1. Notably, the three scanning setups differed with respect to sampling rate (repetition time, TR) and magnetic field strength. Datasets 1 and 2 were acquired using typical EPI-BOLD sequence with 3 T and 1.5 T scanners, respectively. As noted above, dataset 1 also included follow-up imaging up at baseline and at six and 12 months.

fMRI from dataset 3 was acquired with magnetic resonance encephalography (MREG) sequence, which is a three-dimensional (3D) spiral, single shot sequence that undersamples 3D k-space in a spiral trajectory for faster imaging³⁸. The method samples the BOLD signal at 10 Hz frequency, thus 20–25 times faster than in conventional fMRI, such as used in datasets 1 and 2. The high sampling rate of the MREG sequence is crucial to evaluate phenomena in the frequency range of cardiovascular pulsations. While there are a few alternatives for fast sampled fMRI sequences, MREG has been proven suitable to measure physiological pulsations^{32,37}.

Physiological data. For dataset 3 we also collected peripheral heart rate measured using a pulse oximeter (SpO₂ signals from fingertip) and respiratory rate measured using the scanner's respiratory belt. Also, the blood pressure was measured with subjects in a supine position just prior to imaging using GE Datex-Ohmeda Aes-tiva5/MRI compatible anesthesia monitor.

Preprocessing of imaging data. Preprocessing for all three datasets was conducted using the Oxford Centre for Functional MRI of the Brain Software Library 5.0 (FSL 5.0.11, <http://www.fmrib.ox.ac.uk/fsl>)³⁹ exactly as described in²⁷. For fMRI data, the pipeline included head motion correction, brain extraction, spatial smoothing, and high-pass temporal filtering. Multi-resolution affine co-registration within FSL FLIRT software was used to co-register the mean, non-smoothed fMRI and structural maps of corresponding subjects (as described below), and to co-register these volumes to the Montreal Neurological Institute's (MNI152) standard space template. **Motion analysis:** From head motion correction parameters (MCFLIRT), we extracted subject-wise absolute displacement vectors (in mm), which describe the amount of movement in all directions over the entire scan as a marker of gross head motion. Also, relative displacement vectors were extracted, as a marker of motion between each EPI volume. Both vectors were also averaged across volumes to get the mean values. **Structural data and gray matter atrophy (GM) maps:** After visual inspection by an experienced neuroradiologist, structural data was analyzed with FSL-VBM (<http://fsl.fmrib.ox.ac.uk/fsl/fslwiki/FSLVBM>), an optimized VBM protocol executed with FSL tools. First, structural images were skull-stripped and the gray matter was segmented before being registered to the MNI 152 standard space using non-linear plastic registration. The resulting images were averaged and flipped along the x-axis to create a left-right symmetric, study-specific grey matter template. Second, all native grey matter images were non-linearly registered to this study-specific template and "modulated" to correct for local expansion (or contraction) due to the non-linear component of the spatial transformation. The modulated grey matter images were then smoothed with an isotropic Gaussian kernel with a sigma of 3 mm.

Brain signal variability maps (rSD_{BOLD}). For each participant, a map of rSD_{BOLD} was computed as the relative standard deviation of the BOLD timeseries at each voxel from preprocessed functional MRI data:

$$rSD_{BOLD} = \frac{\sigma(X_{BOLD})}{\mu(X_{BOLD})} \quad (1)$$

where X_{BOLD} is voxel time series, σ is the standard deviation and μ is the mean. Representative examples of preprocessed BOLD signals, their standard deviation (SD), mean and the calculated group average rSD_{BOLD} maps are shown in Fig. 1 for all three datasets.

Physiological source mapping (SD_{card} , SD_{resp} and SD_{VLF}). To study the physiological source of BOLD signal variability, we bandpass filtered the critically sampled $MREG_{BOLD}$ signal (dataset 3) to cardiac (>0.6 Hz), respiratory (0.1–0.6 Hz) and very low frequencies (VLF, 0.008–0.1 Hz), using AFNI 3dTProject⁴⁰. For each participant, SD maps of cardiac, respiratory and VLF frequency signals were computed as the standard deviation of the filtered $MREG_{BOLD}$ timeseries at each voxel. Since bandpass filtering removes the signal mean, we here reported standard deviation instead of rSD .

To verify reliability of these signals, average heart and respiratory rates were determined using Fast Fourier Transform from whole brain full band MREG signals. We calculated Pearson's correlation coefficients between these measurements and peripheral heart and respiratory rates measured by the pulse oximeter and respiration belt.

Statistical analysis. All statistical analyses were performed using the GraphPad Prism 8, unless otherwise stated. AD patients were compared to controls in the group-level analysis within each dataset. All results were examined at a $P < 0.05$ significance level, unless otherwise stated. The χ^2 -test was used to calculate P-values for categorical variables and the t-test for continuous variables. **Voxel-level statistical analysis of imaging data:** To examine differences in AD patients versus controls, between-group contrast comparisons of the various parametric maps (GM, rSD_{BOLD} , SD_{card} , SD_{resp} and SD_{VLF}) were statistically tested using permutation-based nonparametric testing incorporating threshold-free cluster enhancement (TFCE) and correction for multiple comparisons implemented in the FSL randomise tool with 10,000 random permutations. In functional data analysis (rSD_{BOLD} and SD maps), relative motion parameters were used as regressors due to the small difference between groups in dataset 1 (Table S2). **Region-of-interests (ROIs):** Statistically significant differences between groups in voxel-level analysis were also used to define region-of-interest (ROI) segments for further analysis. For example, $ROI_{dataset1}$ is defined as the set of voxels with statistically significantly increased rSD_{BOLD} values in the AD group from dataset 1. **Receiver operating characteristic (ROC) curve** and the area under the ROC curve (AUC) were calculated to estimate the feasibility of using rSD_{BOLD} as a potential biomarker for AD. We plotted ROC curves to evaluate whether rSD_{BOLD} could serve to separate healthy controls from patients in datasets 2 and 3. The mean rSD_{BOLD} for each subject was calculated using $ROI_{dataset1}$ (Fig. 2A and 3A), and AUC was calculated as a measure of classification accuracy. The bootstrap approach was used to estimate the 95% confidence interval of AUC. **Follow-up data** in dataset 1 were used to estimate the repeatability and the effect of the disease progression on rSD_{BOLD} . We calculated average rSD_{BOLD} within $ROI_{dataset1}$ for each subject in dataset 1 and plotted this as a function of time. Repeated measures mixed-effect analysis was performed on the follow-up data. Clinical Dementia Rating (CDR) was used as a clinical marker for disease progression to follow-up in the AD group. **Spatial correlation analysis:** To analyze the similarity of the results of different modality voxel-level statistical analysis, we performed spatial cross-correlation correlation of P-value maps of different modalities (rSD_{BOLD} , GM and SD) using the `fsfcc` command of FSL. **Visualization:** Most of the data was plotted using GraphPad Prism 8. Functional MRI data was plotted using Matlab (Fig. 1) or MRICroGL (Fig. 2–4, <https://www.mccau.slandcenter.sc.edu/mricrogl/>).

Data availability

The data that support the findings of this study are available from the corresponding author, upon reasonable request.

Received: 4 August 2020; Accepted: 13 November 2020

Published online: 09 December 2020

References

- Cummings, J. L. Alzheimer's disease. *N. Engl. J. Med.* **351**, 56–67 (2004).
- Selkoe, D. J. & Hardy, J. The amyloid hypothesis of Alzheimer's disease at 25 years. *EMBO Mol. Med.* **8**, 595–608 (2016).
- Chen, G. F. Amyloid beta: structure, biology and structure-based therapeutic development. *Acta Pharmacol. Sin.* **38**, 1205–1235 (2017).
- van der Kant, R., Goldstein, L. S. B. & Ossenkoppele, R. Amyloid- β -independent regulators of tau pathology in Alzheimer disease. *Nat. Rev. Neurosci.* **21**, 21–35 (2020).
- McKhann, G. M. The diagnosis of dementia due to Alzheimer's disease: recommendations from the National Institute on Aging-Alzheimer's Association workgroups on diagnostic guidelines for Alzheimer's disease. *Alzheimer's Dement.* **7**, 263–269 (2011).
- Nadebaum, D. P. A head-to-head comparison of cerebral blood flow SPECT and 18 F-FDG PET in the diagnosis of Alzheimer's disease. *Intern. Med. J. IMJ* <https://doi.org/10.1111/imj.14890> (2020).
- Livingston, G. Dementia prevention, intervention, and care. *The Lancet* **390**, 2673–2734 (2017).
- Park, S. A., Han, S. M. & Kim, C. E. New fluid biomarkers tracking non-amyloid- β and non-tau pathology in Alzheimer's disease. *Exp. Mol. Med.* **52**, 556–568 (2020).
- Brooker, D., Fontaine, J. L., Evans, S., Bray, J. & Saad, K. Public health guidance to facilitate timely diagnosis of dementia: Alzheimer's Cooperative Valuation in Europe recommendations. *Int. J. Geriatr. Psychiatry* **29**, 682–693 (2014).
- Jack, C. R. NIA-AA research framework: toward a biological definition of Alzheimer's disease. *Alzheimer's Dement.* **14**, 535–562 (2018).
- Jung, N. Y. Comparison of diagnostic performances between cerebrospinal fluid biomarkers and amyloid PET in a clinical setting. *J. Alzheimer's Dis.* **74**, 473–490 (2020).
- Agnello, L. Diagnostic accuracy of cerebrospinal fluid biomarkers measured by chemiluminescent enzyme immunoassay for Alzheimer disease diagnosis. *Scand. J. Clin. Lab. Investig.* <https://doi.org/10.1080/00365513.2020.1740939> (2020).
- Williamson, J. D. Effect of intensive vs standard blood pressure control on probable dementia: a randomized clinical trial. *JAMA J. Am. Med. Assoc.* **321**, 553–561 (2019).
- Iliff, J. J. A paravascular pathway facilitates CSF flow through the brain parenchyma and the clearance of interstitial solutes, including amyloid β . *Sci. Transl. Med.* **4**, 147ra111 (2012).
- Aspelund, A. A dural lymphatic vascular system that drains brain interstitial fluid and macromolecules. *J. Exp. Med.* **212**, 991–999 (2015).
- Meng, Y. Glymphatics visualization after focused ultrasound-induced blood-brain barrier opening in humans. *Ann. Neurol.* **86**, 975–980 (2019).
- Kress, B. T. Impairment of paravascular clearance pathways in the aging brain. *Ann. Neurol.* **76**, 845–861 (2014).
- Mestre, H. Flow of cerebrospinal fluid is driven by arterial pulsations and is reduced in hypertension. *Nat. Commun.* **9**, 1–9 (2018).
- Birn, R. M., Diamond, J. B., Smith, M. A. & Bandettini, P. A. Separating respiratory-variation-related fluctuations from neuronal-activity-related fluctuations in fMRI. *Neuroimage* **31**, 1536–1548 (2006).
- Shmueli, K. Low-frequency fluctuations in the cardiac rate as a source of variance in the resting-state fMRI BOLD signal. *Neuroimage* **38**, 306–320 (2007).
- Liu, T. T. Noise contributions to the fMRI signal: an overview. *Neuroimage* **143**, 141–151 (2016).
- Kiviniemi, V. Ultra-fast magnetic resonance encephalography of physiological brain activity-Glymphatic pulsation mechanisms?. *J. Cereb. Blood Flow Metab.* **36**, 1033–1045 (2016).
- Hussein, A. The association between resting-state functional magnetic resonance imaging and aortic pulse-wave velocity in healthy adults. *Hum. Brain Mapp.* <https://doi.org/10.1002/hbm.24934> (2020).
- Makedonov, I., Chen, J. J., Masellis, M. & MacIntosh, B. J. Physiological fluctuations in white matter are increased in Alzheimer's disease and correlate with neuroimaging and cognitive biomarkers. *Neurobiol. Aging* **37**, 12–18 (2016).
- Scarapicchia, V., Mazerolle, E. L., Fisk, J. D., Ritchie, L. J. & Gawryluk, J. R. Resting state BOLD variability in Alzheimer's disease: a marker of cognitive decline or cerebrovascular status?. *Front. Aging Neurosci.* **10**, 39 (2018).
- Jahanian, H. Spontaneous BOLD signal fluctuations in young healthy subjects and elderly patients with chronic kidney disease. *PLoS ONE* **9**, e92539 (2014).
- Tuovinen, T. The effect of gray matter ICA and coefficient of variation mapping of BOLD data on the detection of functional connectivity changes in Alzheimer's disease and bvFTD. *Front. Hum. Neurosci.* **10**, 680 (2017).
- Kananen, J. Altered physiological brain variation in drug-resistant epilepsy. *Brain Behav.* **8**, e01090 (2018).
- Arvanitakis, Z., Shah, R. C. & Bennett, D. A. Diagnosis and management of dementia: review. *JAMA - J. Am. Med. Assoc.* **322**, 1589–1599 (2019).
- Clark, C. M. Variability in annual mini-mental state examination score in patients with probable Alzheimer disease: a clinical perspective of data from the consortium to establish a registry for Alzheimer's disease. *Arch. Neurol.* **56**, 857–862 (1999).
- Posse, S. High-speed real-time resting-state fMRI using multi-slab echo-volumar imaging. *Front. Hum. Neurosci.* <https://doi.org/10.3389/fnhum.2013.00479> (2013).
- Raitamaa, L. Breath hold effect on cardiovascular brain pulsations—a multimodal magnetic resonance encephalography study. *J. Cereb. Blood Flow Metab.* **39**, 2471–2485 (2019).
- Rasmussen, M. K., Mestre, H. & Nedergaard, M. The glymphatic pathway in neurological disorders. *Lancet Neurol.* **17**, 1016–1024 (2018).
- Da Mesquita, S., Fu, Z. & Kipnis, J. The meningeal lymphatic system: a new player in neurophysiology. *Neuron* **100**, 375–388 (2018).
- Fultz, N. E. Coupled electrophysiological, hemodynamic, and cerebrospinal fluid oscillations in human sleep. *Science (80-)* **366**, 628–631 (2019).
- Huotari, N. Sampling rate effects on resting state fMRI metrics. *Front. Neurosci.* **13**, 279 (2019).
- Rajna, Z. 3D multi-resolution optical flow analysis of cardiovascular pulse propagation in human brain. *IEEE Trans. Med. Imaging* **38**, 2028–2036 (2019).
- Assländer, J. Single shot whole brain imaging using spherical stack of spirals trajectories. *Neuroimage* **73**, 59–70 (2013).
- Smith, S. M. Advances in functional and structural MR image analysis and implementation as FSL. *NeuroImage* **23**, S208–S219 (2004).
- Cox, R. W. AFNI: software for analysis and visualization of functional magnetic resonance neuroimages. *Comput. Biomed. Res.* **29**, 162–173 (1996).

Acknowledgments

General: We would like to thank all the participants and their families for their generous support to our research. We acknowledge manuscript editing by Inglewood Biomedical Editing. The authors wish to acknowledge CSC—IT Center for Science, Finland, for computational resources. Data used in preparation of this article were obtained from the Alzheimer’s Disease Neuroimaging Initiative (ADNI) database (adni.loni.usc.edu). As such, the investigators within the ADNI contributed to the design and implementation of ADNI and/or provided data but did not participate in analysis or writing of this report. A complete listing of ADNI investigators can be found at: http://adni.loni.usc.edu/wp-content/uploads/how_to_apply/ADNI_Acknowledgement_List.pdf.

Author contributions

T.T. and V.Ki. designed the study. T.T., J.K., V.Ko., R.R., H.M., H.H., N.H., L.R., A.A.E., J.Kr. and V.Ki. collected the data. T.T., J.Ka., N.H., V.Ko., V.Ki. performed data preprocessing. T.T., V.Ki., J.Ka., V.Ko. performed data analysis. T.T. created figures. T.T., J.Ka., Z.R., J.L., V.Ko., P.L., O.T., J.H., A.M.R., M.N., and V.Ki. interpreted results. All authors discussed the results and contributed to the final manuscript. The investigators within the ADNI contributed to the design and implementation of ADNI and/or provided data but did not participate in analysis or writing of this report.

Funding

This work was supported by grants from Finnish Academy grants 275352, 314497 (V.Ki.), Jane and Aatos Erkko Foundation (V.Ki.), KEVO grants from Oulu University Hospital (V.Ki.), DFG cluster BrainLinks-BrainTools EXC-1086 (P.L.), Epilepsy Research Foundation (J.Ka.), Finnish Cultural Foundation, North Ostrobothnia Regional Fund (J.Ka.), Orion Research Foundation sr (J.Ka., T.T.), Tauno Tönnö Foundation (J.Ka.). The University of Oulu Scholarship Foundation (J.Ka.), Medical Research Center (MRC)-Oulu (J.Ka.), Maire Taponen Foundation sr (J.Ka.), Finnish Brain Foundation sr (J.Ka.), Instrumentarium Science Foundation sr (J.Ka.), The Finnish Medical Foundation (J.L., T.T.), Yrjö Jahnsson’s Foundation (J.L.), The Finnish Medical Society Duodecim Oulu (T.T.). Data collection and sharing for this project was funded by the Alzheimer’s Disease Neuroimaging Initiative (ADNI) (National Institutes of Health Grant U01 AG024904) and DOD ADNI (Department of Defense award number W81XWH-12-2-0012). ADNI is funded by the National Institute on Aging, the National Institute of Biomedical Imaging and Bioengineering, and through generous contributions from the following: AbbVie, Alzheimer’s Association; Alzheimer’s Drug Discovery Foundation; Araclon Biotech; BioClinica, Inc.; Biogen; Bristol-Myers Squibb Company; CereSpir, Inc.; Cogstate; Eisai Inc.; Elan Pharmaceuticals, Inc.; Eli Lilly and Company; EuroImmun; F. Hoffmann-La Roche Ltd and its affiliated company Genentech, Inc.; Fujirebio; GE Healthcare; IXICO Ltd.; Janssen Alzheimer Immunotherapy Research & Development, LLC.; Johnson & Johnson Pharmaceutical Research & Development LLC.; Lumosity; Lundbeck; Merck & Co., Inc.; Meso Scale Diagnostics, LLC.; NeuroRx Research; Neurotrack Technologies; Novartis Pharmaceuticals Corporation; Pfizer Inc.; Piramal Imaging; Servier; Takeda Pharmaceutical Company; and Transition Therapeutics. The Canadian Institutes of Health Research is providing funds to support ADNI clinical sites in Canada. Private sector contributions are facilitated by the Foundation for the National Institutes of Health (www.fnih.org). The grantee organization is the Northern California Institute for Research and Education, and the study is coordinated by the Alzheimer’s Therapeutic Research Institute at the University of Southern California. ADNI data are disseminated by the Laboratory for Neuro Imaging at the University of Southern California.

Competing interests

The authors declare no competing interests.

Additional information

Supplementary information is available for this paper at <https://doi.org/10.1038/s41598-020-77984-1>.

Correspondence and requests for materials should be addressed to T.T. or V.K.

Reprints and permissions information is available at www.nature.com/reprints.

Publisher’s note Springer Nature remains neutral with regard to jurisdictional claims in published maps and institutional affiliations.



Open Access This article is licensed under a Creative Commons Attribution 4.0 International License, which permits use, sharing, adaptation, distribution and reproduction in any medium or format, as long as you give appropriate credit to the original author(s) and the source, provide a link to the Creative Commons licence, and indicate if changes were made. The images or other third party material in this article are included in the article’s Creative Commons licence, unless indicated otherwise in a credit line to the material. If material is not included in the article’s Creative Commons licence and your intended use is not permitted by statutory regulation or exceeds the permitted use, you will need to obtain permission directly from the copyright holder. To view a copy of this licence, visit <http://creativecommons.org/licenses/by/4.0/>.

© The Author(s) 2020